PROCEEDINGS OF ECOS 2023 - THE 36TH INTERNATIONAL CONFERENCE ON
EFFICIENCY, COST, OPTIMIZATION, SIMULATION AND ENVIRONMENTAL IMPACT OF ENERGY SYSTEMS
25-30 JUNE, 2023, LAS PALMAS DE GRAN CANARIA, SPAIN

Concept of the non-equilibrium multi-dimensional model of the charging/discharging low-temperature thermochemical storage unit

Mateusz Młynarczyk[a], Piotr Łapka[b], Natalia Mikos-Nuszkiewicz[c] and Piotr Furmański[d]

[a] *Faculty of Power and Aeronautical Engineering, Warsaw University of Technology, Warsaw, Poland, e-mail: mateusz.mlynarczyk2.stud@pw.edu.pl*
[b] *Faculty of Power and Aeronautical Engineering, Warsaw University of Technology, Warsaw, Poland, e-mail: piotr.lapka@pw.edu.pl*
[c] *Faculty of Power and Aeronautical Engineering, Warsaw University of Technology, Warsaw, Poland, e-mail: natalia.mikos.dokt@pw.edu.pl*
[d] *Faculty of Power and Aeronautical Engineering, Warsaw University of Technology, Warsaw, Poland, e-mail: piotr.furmanski@pw.edu.pl*

Abstract:

Thermochemical energy storage is the least investigated thermal energy storage technology. Nowadays, research on this technology's development is very intensive, including high, medium, and low-temperature applications. However, for thermochemical energy storage technology to get market maturity, still many problems must be solved, and reliable design and optimization tools must be developed. The concept of such a tool, i.e., the multi-dimensional numerical model of the charging/discharging low-temperature thermochemical storage unit, is presented in this paper. The model considers hydration/dehydration reactions in the thermochemical medium working in the open system. It accounts for local hygric and thermal non-equilibrium at the macroscale by treating heat and moisture carrier fluid (moist air) and reactive porous bed separately. Therefore, two sets of governing equations have been derived, i.e., one dealing with moisture and heat transfer in the air flowing through the porous bed and the second one with phenomena occurring in the reactive porous bed. The model assumes regular regimes of heat conduction and moisture diffusion in the bed particles and a fast sorption/desorption rate in thermochemical materials. Moreover, it is assumed that the water removal from the bed particle surface controls the chemisorption process as being slower than reaction kinetics. The proposed model was simplified to heat storage using sorption/desorption phenomena and implemented in 2D axisymmetric space using commercial software. Such an approach allows for easy adjustment and modification of the reactor geometry in the design and optimization path. Then the model in simplified form was applied for the simulation of a sorption-based thermal energy storage unit. Parts of the charging and discharging phases were simulated. However, the long simulation time is the particular issue limiting the current broader testing and applications of the model.

Keywords:

Thermochemical energy storage; Hydration/dehydration; Numerical modeling; Non-equilibrium model; Sorption/desorption;

1. Introduction

To date, global energy consumption significantly relies on fossil fuels which are closely related to carbon dioxide (CO_2) emissions, contributing to climate change. Increasing global energy demands caused by rapid industrialization and population growth and, therefore, acceleration of fossil fuel depletion and the additional need for environmental protection attracts attention to the effective use of the other available energy sources, including renewable ones. These sources often deliver energy in times and locations different from its demand. This leads to an economically unjustified loss of useful energy.

The crucial role of energy storage systems is to reduce the time or rate of mismatch between energy supply coming from different sources and energy demand at a specific time and location. Among the energy storage systems, thermal energy storage (TES) is an important energy conservation technology to store heat and cold for later use [1]. Thermal energy can be stored as sensible heat, latent heat, and thermochemical energy or combinations of these methods [2]. Much research and development work has been carried out in the first two methods of the TES. The sensible heat storage associated with increased temperature of the storing material

https://doi.org/10.52202/069564-0210

is used in many domestic and industrial applications. The method requires a high heat capacity of the storing materials and very good thermal insulation of the storage system to reduce heat losses. These two features are the most significant drawbacks and limitations of sensible heat storage. The latent heat storage uses phase transformations associated with the absorption or release of heat during, e.g., melting/freezing. Therefore, it needs phase change materials (PCMs) of high latent heat and good thermal transport properties to effectively transfer heat to and from the storage. This storage technology has many lab-scale and market applications, including PCM in storage tanks [3] and in different elements of building envelopes [4-7]. However, the drawback of this storage technology, among others, is the low thermal conductivity of PCMs, which significantly limits the heat transfer rates during charging/discharging and heat storing at temperatures different than the temperature of the surroundings and related heat losses. Thermochemical energy storage (TChES) is one of the least investigated heat storage methods. However, it is the most promising and attractive technology because it offers the highest energy storage density of the three methods and allows for storing thermal energy at negligible heat loss for a long time by species separation [2]. Another difference between PCM-based storage and TChES in which gaseous product appears is that the former depends on temperature only, while the latter has an extra control parameter, namely the gas pressure, which follows from the equilibrium curve in the phase diagram of thermochemical material [8]. Recent developments in low/zero energy buildings promote the development of low-temperature TChES systems.

Mathematical models of TES units/systems using sorption and chemical reactions pose many difficulties in mathematical formulations and equations solutions. These processes are complicated and differ from the well-known and analyzed classical flow phenomena with heat transfer. In the TChES, it is required to simultaneously deal with the fluid flow and heat and mass transfer in the porous bed accompanied by sorption or chemical reactions, the dynamics of which also affect the system's operation [9]. Due to the large number of physical phenomena that need to be modeled and the need to combine equations that describe fluid flow, thermal, and chemical processes, modeling these phenomena was significantly simplified.

Several numerical approaches have been proposed to investigate the heat and mass transfer processes in the reactive packed bed and in the whole TChES units/systems. The most simplified are purely thermodynamic approaches based on energy and exergy methods to assess the closed or open-loop TChES systems/units [10, 11] or reaction cycles for the TChES systems/units [12]. The second group of the models is lumped-element or 0D models [13, 14], which provide general information on the TChES unit/systems operation. The next group is the 1D models, which can simulate the variation of the working medium and reactor parameters along the flow path [2, 9, 15, 16]. The most complex approaches are multi-dimensional (2 and 3D) models [17-21] capable of predicting fluid flow and thermal and chemical states at any time of the process and any point in the storage unit/system and, therefore, are applied for multi-criteria analyses of TChES units/systems.

Most of the TChES units/systems models assumed many simplifications. For example, local thermal equilibrium between working gas and the porous bed was applied [17-19, 21], the gas flow was modeled as isothermal [17-19], the flow of the gas in the porous bed was evaluated through Darcy law [17-19, 21], vapor transfer dynamics was omitted [17-21]. These simplifications are understandable and justified. The phenomena controlling the TChES process are very complex, and their modeling requires many assumptions to solve the problem. However, this paper will try to alleviate some of the mentioned assumptions by treating simplified or omitted phenomena more rigorously than in the previous works [17-21]. The proposed new 2D macroscale model, based on the previous 1D approach [9], considers low-temperature hydration/dehydration reactions in the TChES unit working in the open system. It assumes hygric and thermal non-equilibrium between the working medium (moist air) and the reactive porous bed and, in this way, accounts for the peculiarities and dynamics of heat and mass transfer processes in a porous bed. The model may be applied to simulate the chemical and physical sorption-based storage process.

2. Macroscopic mathematical model of TChES unit

This chapter contains a description of the complex TChES unit model. The model consists of the unsteady equations set describing the transport of momentum, mass, energy, and moisture in the gaseous phase and the transport of energy and moisture in the solid phase (porous bed). The first equation, i.e., the continuity equation for moist air in the storage, is written as follows:

$$\varepsilon_b \frac{\partial \rho_m}{\partial t} + \nabla \cdot (\rho_m \vec{u}) = 0, \tag{1}$$

where: ρ_m is the moist air density, ε_b is the reactive bed porosity, $\vec{u}$ is the velocity vector, and t is the time. The laminar flow was assumed to simplify the case. Therefore, the momentum equation is the following:

$$\frac{\partial \rho_m}{\partial t} + \nabla \cdot (\rho_m \vec{u}\vec{u}) = -\nabla p + \nabla \cdot \mu_m \left[(\nabla \vec{u} + \nabla \vec{u}^T) - \frac{2}{3} \nabla \cdot \vec{u} I \right] - \frac{\mu_m}{k} \vec{u} + C_2 \frac{1}{2} \rho_m |\vec{u}| \vec{u}. \tag{2}$$

In the equation above, p is the static pressure, I is the unit tensor, and μ_m is the moist air dynamic viscosity. The two last terms of Eq. (2) are source terms accounting for the porous zone region. The factor k is the permeability of the reactive bed, and coefficient C_2 is used to include inertial pressure losses. The moisture

https://doi.org/10.52202/069564-0210

must be properly managed in the reactive bed for proper storage work. During the charging cycle, dry air flowing through the bed should remove moisture from the system. In the discharging cycle, the moisture is supplied to the system as water vapor in the moist air. The following non-equilibrium equation describes the moisture transport in the air in a porous bed:

$$\varepsilon_b \frac{\partial \rho_g \omega}{\partial t} + \nabla \cdot \left(\rho_g \vec{u} \omega\right) = \nabla \cdot \left(D_{vb,eff} \nabla \omega\right) + A_b \alpha_{m,eff} \left(\rho_{v,e} - \rho_v\right), \tag{3}$$

where: ρ_g is the density of dry air, ω is the specific humidity (per mass of dry air), $D_{vb,eff}$ is effective vapor diffusivity in air, A_b is the specific surface area of the porous bed, $\alpha_{m,eff}$ is the effective mass transfer coefficient for water vapor, $\rho_{v,e}$ is equilibrium density of water vapor at the surface of bed particles, and ρ_v is the density of the water vapor in moist air. The non-equilibrium thermal model is applied to account for the porous zone's energy transport. The source term in the energy equation includes heat transport between the bed and gaseous phase and the energy transport caused by moisture exchange. Therefore, the energy equation for the moist air is written as:

$$\varepsilon_b \frac{\partial \rho_g \left(c_{v,g} + \omega c_{v,v}\right) T_f}{\partial t} + \nabla \cdot \left[\rho_g \vec{u} \left(c_{p,g} T_f + \omega c_{p,v} T_f + \frac{p}{\rho_g}\right)\right] = \nabla \cdot \left(\lambda_{m,eff} \nabla T_f\right) +$$

$$A_b \left[\alpha_{m,eff} c_{p,v} \left(\rho_{v,e} - \rho_v\right) + \alpha_{T,eff}\right] \left(T_s - T_f\right), \tag{4}$$

where: $c_{v,g}$ and $c_{p,g}$ are the specific heats of dry air at constant volume and pressure, respectively, $c_{v,v}$ and $c_{p,v}$ are the specific heats of vapor at constant volume and pressure, respectively, T_f is the temperature of moist air (working fluid), $\lambda_{m,eff}$ is the effective heat conductivity of moist air, $\alpha_{T,eff}$ is the effective heat transfer coefficient between gaseous phase and solid particles, and T_s is the temperature of the porous reactive bed. In the mass balance equation for the solid phase, the formation of new substances during the chemical reaction is taken into account. It is assumed that water in particles occurs only in the bound state of component A (hydrate). There is no diffusion between hydrated component A and dehydrated component B. Therefore, the mass balance equation can be written as:

$$\left(1 - \varepsilon_b\right) \frac{\partial \left(\rho_A + \rho_B\right)}{\partial t} = -A_b \alpha_{m,eff} \left(\rho_{v,e} - \rho_v\right), \tag{5}$$

where: ρ_A is component A's density and ρ_B is component B's density. The degree of transformation of species A into B varies with the location and time. The equation describing this parameter is the following:

$$\beta(\bar{x}, t) = \frac{C_{A0}(\bar{x}) - C_A(\bar{x}, t)}{C_{A0}}, \tag{6}$$

where: $\bar{x}$ is the position vector, C_{A0} is the initial molar concentration of component A, and C_A is the actual molar concentration of species A. The final expression describing the degree of transformation of species A into B is as follows:

$$\frac{\partial \beta}{\partial t} = \frac{A_b \alpha_{m,eff} \left(\rho_{v,e} - \rho_v\right)}{C_{A0} M_{AB} \left(1 - \varepsilon_b\right)}, \tag{7}$$

where M_{AB} is defined as:

$$M_{AB} = M_A - \frac{v_B}{v_A} M_B. \tag{8}$$

In the equation above, M_A is the molar mass of component A, M_B is the molar mass of component B, and v_A and v_B are stoichiometric coefficients. The energy equation for solid particles considers the heat and mass exchange with flowing air and energy released (or absorbed) during the chemical reaction. Therefore, this energy equation can be written using the formula:

$$\left(1 - \varepsilon_b\right) \left[\frac{v_B}{v_A} \frac{\partial H_B}{\partial T_s} + \left(1 - \beta\right) \frac{\partial H_{AB}}{\partial T_s}\right] = \nabla \cdot \left(\lambda_{s,eff} \nabla T_s\right) +$$

$$-A_b \left[\alpha_{m,eff} c_{p,v} \left(\rho_{v,e} - \rho_v\right) + \alpha_{T,eff}\right] \left(T_s - T_f\right) + \left(1 - \varepsilon_b\right) H_{AB}(T_s) \frac{\partial \beta}{\partial t}, \tag{9}$$

where H_{AB} is defined as:

$$H_{AB} = H_A - \frac{v_B}{v_A} H_B. \tag{10}$$

In Eq. (9) and (10), H_A is species A's molar enthalpy, H_B is species B's molar enthalpy, and $\lambda_{s,eff}$ is the effective heat conductivity of solid particles in the reactive bed. Equations (1)-(10) allow for calculating velocities, temperatures, and moisture molar concentration fields. Due to the high complexity of the proposed model, caused by the presence of chemical reaction in the bed and the coexistence of both species A and B, the above model was simplified and reformulated to account for a sorption/desorption-based heat storage, which mathematical description is much simpler, and in such form was implemented and tested. The model given by Eq. (1)-(10) will be implemented and tested in future work.

3. Model simplification to sorption/desorption-based heat storage

The proposed in section 2 TChES model was simplified, assuming that sorption/desorption phenomena are used to store heat instead of thermochemical reactions. The simplified mathematical model for sorption/desorption-based heat storage, presented below, replaces the mass balance equation, Eq. (5), with the equation describing water transport in the porous bed. It assumes that, during the sorption, the water vapor is adsorbed from moist air and bound with solid porous particles in liquid form. No other species are created in the bed because only physical adsorption occurs. Therefore, the density of the solid phase is constant, and the mass changes of particles arise only from the amount of adsorbed water. The following equation can describe the sorption phenomenon:

$$(1-\varepsilon_b)\rho_s \frac{\partial a_w}{\partial t} = (1-\varepsilon_b)\rho_s A_b \alpha_{m,eff}\left(a_{w,eq} - a_w\right), \tag{11}$$

where: ρ_s is the real density of solid particles, a_w is the mass of adsorbed water (per mass of adsorbent particles), and $a_{w,e}$ is the equilibrium amount of water. Both sides of Eq. (11) are multiplied by the mass of the adsorbent per volume to obtain the SI unit compatible with the moisture transport equation for moist air, i.e., kg H_2O m^{-3} s^{-1}. The source term of Eq. (3) also was changed because of replacing the driving force of water transfer. It is assumed that there will not be condensation, and water in the system occurs only in the form of water vapor in moist air and water adsorbed by porous particles. Therefore, Eq. (3) and (11) have the opposite source terms. The modified equation of moisture transport in the air is the following:

$$\varepsilon_b \frac{\partial \rho_g \omega}{\partial t} + \nabla \cdot \left(\rho_g \vec{u} \omega\right) = \nabla \cdot \left(D_{vb,eff} \nabla \omega\right) + (1-\varepsilon_b)\rho_s A_b \alpha_{m,eff}\left(a_w - a_{w,eq}\right). \tag{12}$$

In the energy equation for the moist air, Eq. (4), the only change will occur in the source term connected with energy transport as enthalpy of exchanged water. The modified equation can be written as:

$$\varepsilon_b \frac{\partial \rho_g \left(c_{v,g} + \omega c_{v,v}\right) T_f}{\partial t} + \nabla \cdot \left[\rho_g \vec{u} \left(c_{p,g} T_f + \omega c_{p,v} T_f + \frac{p}{\rho_g}\right)\right] = \nabla \cdot \left(\lambda_{m,eff} \nabla \mathrm{T}_f\right) +$$

$$A_b\left[(1-\varepsilon_b)\rho_s \alpha_{m,eff} c_{p,v}\left(a_w - a_{w,eq}\right) + \alpha_{T,eff}\right]\left(T_s - T_f\right). \tag{13}$$

The energy equation for the porous bed in the simplified model considers the specific heat of adsorbed water in porous particles and the heat of sorption. Therefore, the energy Eq. (9), is replaced by the following one:

$$\rho_s (1-\varepsilon_b) \frac{\partial \left(c_{p,s} + a_w c_{p,\mathrm{H2O}}\right) T_s}{\partial t} = \nabla \cdot \left(\lambda_{s,eff} \nabla \mathrm{T}_s\right) + (1-\varepsilon_b)\rho_s A_b \alpha_{m,eff}\left(a_{w,eq} - a_w\right) H_r +$$

$$-A_b\left[(1-\varepsilon_b)\rho_s \alpha_{m,eff} c_{p,v}\left(a_w - a_{w,e}\right) + \alpha_{T,eff}\right]\left(T_s - T_f\right), \tag{14}$$

where: $c_{p,s}$ is the specific heat of solid particles, $c_{p,\mathrm{H2O}}$ is the specific heat of liquid water, and H_r is the heat of sorption reaction (per mass of exchanged water). Flow equations, Eq. (1) and (2), remained the same in the simplified model.

4. Numerical implementation

4.1. Storage unit geometry and mesh

The sorption/desorption TES unit of cylindrical shape is investigated. During the modeling of the TES unit, the focus was not only on processes occurring in the porous medium but also on the part through which the air reached the reactive bed and flowed out of it. The 2D geometry of the modeled part of the TES unit consists of a circular inlet channel, a diverging nozzle, a cylindrical reactor with a porous material, a converging nozzle, and an outlet channel (see Figure 1). This geometry is axisymmetrical.

The axial symmetry of the geometry enabled a significant reduction in the number of mesh elements by treating the problem as a 2D axisymmetric. Consequently, only the upper part of the axial section needs to be prepared and meshed. A detailed view of the storage geometry with all dimensions is presented in Figure 2. The geometry of the TES unit was created using the ANSYS DesignModeler software.

https://doi.org/10.52202/069564-0210

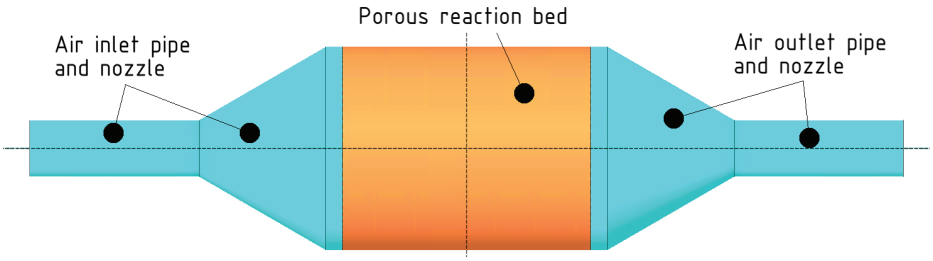

Figure. 1. The schematic view of investigated sorption/desorption TES unit.

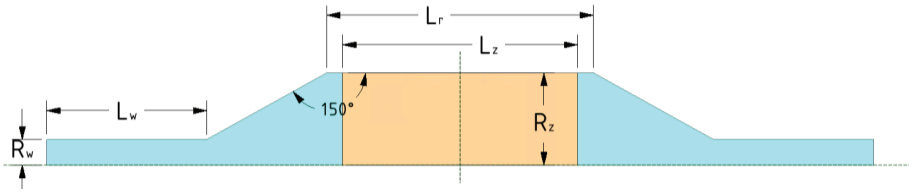

Figure. 2. The view of the upper axial section of the TES unit with all dimensions.

Table 1. Geometric dimensions of the investigated TES unit.

Geometrical parameters	Value
R_w (m)	0.05
R_z (m)	0.18
L_w (m)	0.30
L_r (m)	0.50
L_z (m)	0.44
Inlet/outlet surface (cm^2)	78.54
System volume (dm^3)	76.31
Reactive bed volume (dm^3)	44.79

Table 2. Mesh elements' quality properties.

Element property	Mesh 1 (15 680 elements)	Mesh 2 (273 570 elements)
Maximum aspect ratio	11.35	11.38
Minimum orthogonal quality	0.84	0.86
Maximum skewness	0.33	0.33

The TES unit's regular geometry allowed to generate meshes with 2D quadrangular elements. The meshes were created using the ANSYS Meshing software. Two computational grids, i.e., coarse and dense, were considered for testing the model's stability and solution sensitivity to the mesh size. The equations' convergence levels were also checked. Three factors were considered, i.e., aspect ratio, orthogonal quality, and skewness, to assess the quality of grid elements. As seen from the data presented in Table 2, the qualities of meshes are very good. During grids generations, refined meshes were created at the pipe and nozzle walls, thanks to which processes occurring in the boundary layers were simulated more accurately. For this reason, the aspect ratio level close to the walls was higher than in the rest of the domain. The reactive bed is the region with the best quality elements to decrease the meshing impact on equations convergence rates.

The coarse and dense meshes comprised 15 680 and 273 570 elements, respectively. But, this is not the final element numbers ANSYS Fluent used during the solution. Since a non-equilibrium approach was applied in solving the energy equation in the porous zone, ANSYS Fluent required a copy of the mesh in the porous region. The copied mesh consisted of the same number of elements as in the area of the porous medium, but these elements belonged to the solid material and used solid material properties during calculations. In this work, these were the properties of silica gel. The final sizes of meshes used for calculations were 21 344 and 346 170 elements. Because meshes in the porous media were copied, the elements' quality did not change.

4.2. Numerical implementation

The ANSYS Fluent 2022 R2 software was applied to solve the set of governing equations, Eq. (1), (2), and (11)-(14), utilizing parallel calculations. For the mesh with 21 344 elements, 4 computational nodes were used, and in the case of 346 170 mesh elements, 16 computational nodes were involved. Equations (1) and (2) were solved using a laminar flow model built-in within ANSYS Fluent software. The advanced customization interface, i.e., user-defined scalars (UDS), user-defined functions (UDF), and user-defined memory (UDM),

were applied to solve Eq. (11)-(14), along with all closing relationships presented in the next section. The model implementation using ANSYS Fluent software makes changing the geometry and computational mesh very easy, allowing for future optimization of the TES unit performance.

4.3. Closing relationships and input data

Several closing relationships and a set of input data are required to solve governing equations, Eq. (1), (2), and (11)-(14). These are the following. The density of the dry air in the system was calculated with the following incompressible ideal gas model:

$$\rho_g = \frac{p_{op}}{R_g T_f}, \tag{15}$$

where: p_{op} is the operating pressure assumed constant, and R_g is the individual gas constant of dry air. The density of the moist air changes with the amount of water vapor contained and is calculated using the relation:

$$\rho_m = \rho_g \frac{1+\omega}{1+\frac{R_v}{R_g}\omega}, \tag{16}$$

where: R_v is the individual gas constant of water vapor. The moist air's dynamic viscosity also varies with the contained water vapor as follows:

$$\mu_m = \mu_g + \left(\mu_v - \mu_g\right)\frac{\omega}{\frac{M_v}{M_g}+\omega}, \tag{17}$$

where: μ_g is the dynamic viscosity of the dry air, μ_v is the dynamic viscosity of water vapor, and M_g and M_v are molar masses of dry air and water vapor, respectively. The permeability of a porous medium composed of spherical particles can be calculated using a relationship that considers the grain diameter and the porosity of a given medium. The formula is the following:

$$k = \frac{d_p^2 \varepsilon_b^3}{150(1-\varepsilon_b)^2}, \tag{18}$$

where d_p is the diameter of the particle, i.e., silica gel granules. The coefficient of inertial resistance must be found to calculate the source term of the momentum equation in a porous medium. This coefficient can be calculated using the following formula:

$$C_2 = \frac{2C_F}{\sqrt{k}}, \tag{19}$$

where C_F is the dimensionless Forchheimer drag coefficient. This coefficient value can also be found based on the diameter of the silica gel granules and the porosity of the medium from the following equation:

$$C_F = \frac{1.75}{\sqrt{150}}\varepsilon_b^{-\frac{3}{2}}. \tag{20}$$

A model that considers the bed's porosity, tortuosity, and current air humidity is applied to find the effective diffusivity of moisture in the air in the reactive bed. The reference diffusivity was the one of water vapor in the atmospheric air, which depends only on the air temperature and is described by the following equation:

$$D_{v,a} = 2.6 \cdot 10^{-5}\left(\frac{T_f}{298}\right)^{\frac{3}{2}}. \tag{21}$$

Then the effective diffusivity of vapor in the air in the porous bed was calculated from the following relationship:

$$D_{vb,eff} = \frac{\rho_g D_{v,a}\varepsilon_b}{(1+\omega)\tau_b}, \tag{22}$$

where τ_b is the tortuosity of the bed. The effective thermal conductivity of the porous material was modeled with a simple equation in which the thermal conductivity between the bed's granules depends on the medium's porosity. The equation describing this conductivity can be written as follows:

$$\lambda_{s,eff} = (1-\varepsilon_b)\lambda_s, \tag{23}$$

where: λ_s is the real thermal conductivity of the solid material. The thermal conductivity of moist air was modeled similarly to the dynamic viscosity (see Eq. (17)) using the following equation:

$$\lambda_m = \lambda_g + \left(\lambda_v - \lambda_g\right)\frac{\omega}{\frac{M_v}{M_g}+\omega}, \tag{24}$$

https://doi.org/10.52202/069564-0210

where: λ_g is the thermal conductivity of the dry air, and λ_v is the thermal conductivity of water vapor. The effective thermal conductivity of moist air was modeled in a similar way to the effective conductivity of silica gel, and the equation that describes it is the following:

$$\lambda_{m,eff} = \varepsilon_b \lambda_m. \tag{25}$$

The specific surface area for a bed that consists entirely of spherical grains can be expressed as follows:

$$A_b = \frac{6(1-\varepsilon_b)}{d_p}. \tag{26}$$

The effective heat transfer coefficient was calculated assuming a regular regime and was based on dimensionless relations containing similarity numbers. The equation describing this coefficient can be written in the following form:

$$\alpha_{T,eff} = \frac{\alpha_T}{\sqrt{\mathrm{Bi}_T{}^2 + 1.437\mathrm{Bi}_T + 1}}, \tag{27}$$

where: α_T is the heat transfer coefficient, and Bi_T is the thermal Biot number. This Biot number can be calculated using the following formula:

$$\mathrm{Bi}_T = \frac{\alpha_T L_c}{\lambda_{p,ef}}, \tag{28}$$

where: L_c is the solid particle characteristic length, and $\lambda_{p,ef}$ is the effective thermal conductivity of the grains. The solid particle characteristic length can be found using the following relationship:

$$L_c = \frac{3d_p}{2\pi^2}. \tag{29}$$

The effective thermal conductivity of the grain is the average value between the minimum and maximum thermal conductivity in the porous particle expressed by the following formula:

$$\lambda_{p,ef} = \frac{1}{2}\left\{\left(1-\varepsilon_p\right)\lambda_s + \varepsilon_p\lambda_m + \left[\frac{\left(1-\varepsilon_p\right)}{\lambda_s} + \frac{\varepsilon_p}{\lambda_m}\right]^{-1}\right\}, \tag{30}$$

where ε_p is the porosity of a solid particle. The following Nusselt number correlation was employed to calculate the heat transfer coefficient:

$$\mathrm{Nu}_d = \frac{2.06}{\varepsilon_b}\mathrm{Re}_d^{0.425}\mathrm{Pr}^{\frac{1}{3}}, \tag{31}$$

where: Re_d is the Reynold number, and Pr is the Prandtl number. These dimensionless numbers can be calculated locally (for each mesh cell) with the following formulae:

$$\mathrm{Re}_d = \frac{\rho_m u d_p}{\mu_m}, \tag{32}$$

$$\mathrm{Pr} = \frac{\mu_m\left(c_{p,g} + \omega c_{p,v}\right)}{\lambda_m}. \tag{33}$$

The Nusselt number allows finding the heat transfer coefficient using its following definition:

$$\alpha_T = \frac{\mathrm{Nu}_d \lambda_m}{d_p}. \tag{34}$$

The effective mass transfer coefficient was calculated using the heat and mass transfer analogy by applying the following formula:

$$\alpha_{m,eff} = \frac{\alpha_m}{\sqrt{\mathrm{Bi}_m{}^2 + 1.437\mathrm{Bi}_m + 1}}, \tag{35}$$

where: α_m is the coefficient mass transfer coefficient, and Bi_m is the mass Biot number found using the following relationship:

$$\mathrm{Bi}_m = \frac{\alpha_m L_c}{D_{vp,eff}}, \tag{36}$$

where: $D_{vp,eff}$ is the effective vapor diffusivity in the air filling the porous particle. This effective diffusivity is calculated with the formula:

$$D_{vp,eff} = \frac{D_{va,s}\varepsilon_p}{\tau_p}, \tag{37}$$

where: $D_{va,s}$ is the reference moisture diffusivity calculated by Eq. (21) with the silica gel temperature T_s instead of the moist air temperature, and τ_p is the tortuosity of the solid particle. Formulae similar to those used to determine the heat transfer coefficient were used to calculate the mass transfer coefficient. In these equations, the Sherwood number was used instead of the Nusselt number, and the Schmidt number instead of the Prandtl number. By applying the analogy between heat and mass transfer, the correlation given by Eq. (31) can be modified, obtaining the following one:

$$\mathrm{Sh}_d = \frac{2.06}{\varepsilon_b}\mathrm{Re}_d^{0.425}\mathrm{Sc}^{\frac{1}{3}}. \tag{38}$$

The Schmidt number can be found using the following relation:

$$\mathrm{Sc} = \frac{\mu_m}{\rho_m D_{va,s}}. \tag{39}$$

The Sherwood number allows finding the mass transfer coefficient using its following definition:

$$\alpha_m = \frac{\mathrm{Sh}_d D_{va,s}}{d_p}. \tag{40}$$

Table 3 Fixed physical properties of the model.

Property	Symbol	Value
Porosity of the bed (-)	ε_b	0.6
Porosity of the particle (-)	ε_p	0.6
Diameter of the particle (m)	d_p	0.004
Tortuosity of the bed (-)	τ_b	1000
Tortuosity of the particle (-)	τ_p	1000
Specific heat of dry air at constant volume (J kg^{-1} K^{-1})	$c_{v,g}$	719.53
Specific heat of dry air at constant pressure (J kg^{-1} K^{-1})	$c_{p,g}$	1006.43
Individual gas constant of dry air (J kg^{-1} K^{-1})	R_g	286.9
Thermal conductivity of dry air (W m^{-1} K^{-1})	λ_g	0.0242
Dynamic viscosity of dry air (Pa s)	μ_g	0.000017894
Specific heat of water vapor at constant volume (J kg^{-1} K^{-1})	$c_{v,v}$	1408.5
Specific heat of water vapor at constant pressure (J kg^{-1} K^{-1})	$c_{p,v}$	1870
Individual gas constant of water vapor (J kg^{-1} K^{-1})	R_v	461.5
Thermal conductivity of water vapor (W m^{-1} K^{-1})	λ_v	0.0182
Dynamic viscosity of water vapor (Pa s)	μ_v	0.000010057
Specific heat of liquid water (J kg^{-1} K^{-1})	$c_{p,\mathrm{H2O}}$	4186
Specific heat of solid particles J kg^{-1} K^{-1})	$c_{p,s}$	975
Density of solid particles (kg m^{-3})	ρ_s	2200
Maximum amount of water the silica gel can absorb (-)	$a0$	0.35
Characteristic activation energy (J mol^{-1})	βE	3780.8
Heat of sorption reaction (kJ kg^{-1})	H_r	2415
Correction parameter (-)	n	1.016
Operating pressure (Pa)	p_{op}	101325

The equilibrium moisture content in the solid was modeled based on the Dubinin-Astakhov equation and is expressed by the following formula:

$$a_{w,eq} = a_0 \exp\left[-\left(\frac{A_{ad}}{\beta E}\right)^n \right], \tag{41}$$

where: a_0 is the maximum amount of water the silica gel can absorb, A_{ad} is the adsorption potential coefficient, βE is the characteristic activation energy, and n is the equation parameter. The adsorption potential can be found with the following formula:

$$A_{ad} = BT_f ln\left(\frac{p_{sat}}{p_v}\right), \tag{42}$$

https://doi.org/10.52202/069564-0210

where: B is the universal gas constant, p_v is the pressure of water vapor, and p_{sat} is the saturation pressure of water vapor at temperature T_f calculated by the following expression:

$$p_{sat} = 3567 \exp\left[-5232\left(\frac{1}{T_f} - \frac{1}{300}\right)\right], \tag{43}$$

and the actual water vapor pressure in the moist air can be found by applying the following relationship:

$$p_v = \frac{\omega p}{\frac{M_v}{M_g} + \omega}. \tag{44}$$

Some of the physical properties of moist air (used as the working medium), silica gel (used as the thermochemical material filling the TES unit), and the structure of the porous bed were assumed to be fixed. These properties are listed in Table 3 with their respective descriptions and physical units. Table 4 summarises assumed initial and boundary conditions. Initial conditions were the same for the whole domain. All the walls of the TES units were assumed adiabatic.

Table 4 Initial and boundary conditions for charging and discharging.

Initial and boundary conditions	Symbol	Value (charging/discharging)
Initial velocity of the moist air in the unit (m s^{-1})	u	0 / 0
Initial gauge pressure of the moist air in the unit (Pa)	p	0 / 0
Initial specific humidity in the unit (-)	ω	0.025 / 0.00062
Initial mass of adsorbed water in the unit (-)	a_w	0.32 / 0.035
Initial temperature of moist air in the unit (K)	T_f	303 / 303
Initial temperature of solid particles in the unit (K)	T_s	303 / 303
Inlet velocity of moist air (m s^{-1})	u	2.5 / 2.5
Inlet temperature of moist air (K)	T_f	363 / 293
Inlet specific humidity (-)	ω	0.0095 / 0.0125

5. Results of the simulations

The model validation was not conducted at the current model development state, while model verification was limited to initial mesh size sensitivity analysis and assessing mass and heat conservation principles. But the experimental stand is under development, and the model will be validated in the future. The implemented model was used to simulate the charging and discharging of the sorption-based TES unit. Both simulations were run twice, using a smaller and larger computational grid. A small time step of 0.02 s was used for all tests to improve the equations' convergence rates. Preliminary simulation results were to verify that the implemented numerical model is stable and satisfies the basic mass and energy conservation principles. In addition, it was checked whether the size of the computational grid impacts the calculated characteristics of heat and mass transfer between the reactive bed and moist air. Due to the high complexity of the model, many coupling between equations and other parameters, and the resulting huge demand for computing power, the actual computation times were about a month for TES discharging and another month for charging. For this reason, simulations were stopped at the early stages of the process, and only several minutes of the charging and discharging process were simulated. The simulated charging times on the small and large grids are 2630 s (131 500 time steps) and 632.54 s (31 627 time steps), respectively. For discharge, the simulated times reached 2089.94 s (104 497 time steps) on the small grid and 821.4 s (41 070 time steps) on the large grid.

After the calculations, it was verified whether the implemented model obeyed the basic mass and heat conservation laws at each time step. To do so, the exact amount of masses and energies that were contained, entered, and left the system were recorded after each time step. The energy sources in the system were the entering air and the heat of the sorption reaction. Water was supplied to the system only through moist air. The overall energy balance in the system was calculated in each time step using the following formula:

$$(H_{in} - H_{out}) + H_r = \left(U_{gas}^t - U_{gas}^{t-1}\right) + (U_{sol}^t - U_{sol}^{t-1}), \tag{45}$$

where: H_{in} and H_{out} are entering and leaving air enthalpies, respectively, U_{gas} is the internal energy of air contained in the system, and U_{sol} is the internal energy of solid particles and bounded water. The superscript t means the value taken at the actual time step, while t-1 at the previous time step. Similarly, the water and moist air balances in the system can be written as:

$$\left(m_{w,in} - m_{w,out}\right) = \left(m_{w,gas}^t - m_{w,gas}^{t-1}\right) + \left(m_{w,sol}^t - m_{w,sol}^{t-1}\right), \tag{46}$$

$$\left(m_{a,in} - m_{a,out}\right) = (m_a^t - m_a^{t-1}), \tag{47}$$

where: $m_{w,in}$ and $m_{w,out}$ are the masses of water vapor entering and leaving the system, respectively, $m_{w,gas}$ is the mass of water vapor contained in the system, $m_{w,sol}$ is the mass of water contained in the silica gel bed, $m_{a,in}$ and $m_{a,out}$ are the masses of moist air entering and leaving the system, respectively, and m_a is the mass of moist air contained in the system. The right-hand sides of Eq. (45)-(47) have been moved to the left to simplify the balance evaluation. Thus, properly balanced quantities should take values close to zero.

Table 5 Balances of the energy, the mass of water, and the mass of moist air.

Average residues per time step	Value	Simulation time (s)	Number of grid elements
Average residue of energy during charging (J)	$1.0092 \cdot 10^{-3}$	632.54	21 344
	$4.2618 \cdot 10^{-3}$	632.54	346 170
	$4.0947 \cdot 10^{-5}$	2630	21 344
Average residue of water mass during charging (kg)	$5.0959 \cdot 10^{-12}$	632.54	21 344
	$-1.1001 \cdot 10^{-10}$	632.54	346 170
	$1.1861 \cdot 10^{-10}$	2630	21 344
Average residue of moist air mass during charging (kg)	$1.9798 \cdot 10^{-11}$	632.54	21 344
	$-2.3261 \cdot 10^{-9}$	632.54	346 170
	$3.4112 \cdot 10^{-12}$	2630	21 344
Average residue of energy during discharging (J)	$-7.0426 \cdot 10^{-4}$	821.4	21 344
	$-1.2043 \cdot 10^{-3}$	821.4	346 170
	$-1.7621 \cdot 10^{-4}$	2089.94	21 344
Average residue of water mass during discharging (kg)	$9.2381 \cdot 10^{-13}$	821.4	21 344
	$4.9613 \cdot 10^{-11}$	821.4	346 170
	$3.2810 \cdot 10^{-12}$	2089.94	21 344
Average residue of moist air mass during discharging (kg)	$-1.1574 \cdot 10^{-12}$	821.4	21 344
	$-3.2515 \cdot 10^{-11}$	821.4	346 170
	$5.6194 \cdot 10^{-12}$	2089.94	21 344

Table 6 Differences between results obtained applying a smaller and larger computational grid.

Simulation result	Value	Number of grid elements
Water adsorbed by silica gel during discharging (kg)	0.2261280	21 344
	0.2261438	346 170
Water desorbed by silica gel during charging (kg)	0.1712517	21 344
	0.1712699	346 170
Energy released during the adsorption reaction (J)	546099.10	21 344
	546123.98	346 170
Energy absorbed during the desorption reaction (J)	413572.40	21 344
	413616.44	346 170

The results in Table 5 confirm that the implemented model satisfies the mass and energy conservation principles. Although the residues of the energy equation seem quite large, and after multiplying the average per time step by the number of time steps, the result on the order of magnitude of 100 J was obtained. But this amount is a very small part of the energy released or absorbed during the sorption reaction. For example, the average energy residue per time step during charging was $4.2618 \cdot 10^{-3}$ J, and after 31 627 time steps amounted to 134.79 J. But solid particles absorbed 413 616 J of the heat during the desorption reaction. This means the error is insignificant and does not affect the simulation result.

Next, it was also checked whether the size of the computational grid impacted the simulation result, i.e., the initial mesh sensitivity analysis was performed. For this purpose, differences in the amount of water exchanged between the air and the porous bed as well as stored and released heat in sorption reactions, were checked. The operating period that was considered was 632.54 s of charging and 821.4 s of discharging. As can be seen in Table 6, the size of the computational grid has a very small effect on the simulated amounts of adsorbed and desorbed water as well as absorbed and released heat.

Exemplary simulation results are shown in Figures 3 and 4. However, only the initial charging and discharging phases were simulated due to the long computational times resulting from the model and its implementation complexity. Figure 3 shows how the moisture content of the silica gel granules changed as the TES unit was loaded. It can be seen that dehydration occurs best on the axis of the storage and near its outer wall. Figure 4 shows how the temperature of the moist air in the TES unit changes as it is unloaded. The silica gel granules adsorb water and, as a result, warm up and transfer heat to the flowing air. Here, too, it can be seen that the process is faster at the axis and near the wall of TES. Sorption and heat transfer processes occur fastest in axial and wall regions, most likely due to higher air velocity than in other storage zones. This higher velocity

https://doi.org/10.52202/069564-0210

results in a higher local Reynolds number making mass and heat transfer coefficients more intensive there. The air velocity distribution at the entrance to the porous bed results from the shape of the diffuser before the bed. The air with the highest momentum flows in the axis (the core of the flow), while at the outer walls, vortices are formed just in front of the bed in the central part of the diffuser, which improves mass and energy convection in the bed close to walls.

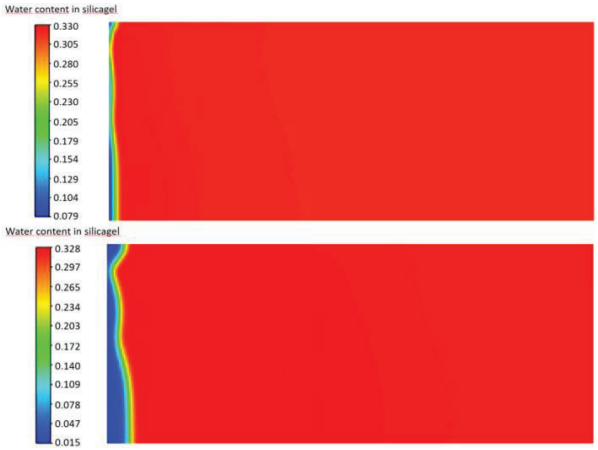

Figure. 3. The contour of water content a_w in silica gel during charging at 2 min (upper) and 10 min (lower) of simulation.

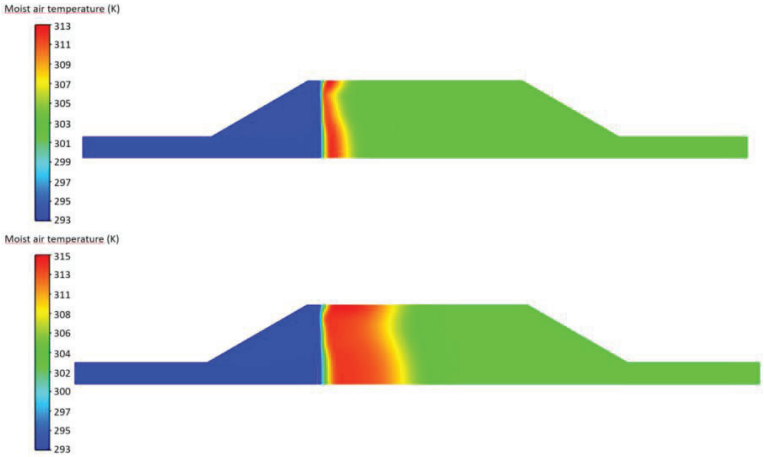

Figure. 4. The contour of moist air temperature during discharging at 2 min (upper) and 10 min (lower) of simulation.

6. Conclusions

The paper presents the concept of an advanced multi-dimensional TChES system model. The model simulates the charging/discharging of a low-temperature TChES unit that operates in an open system. The gaseous working medium (moist air) provides and removes heat and moisture from the unit. The porous thermochemical material stores the heat due to hydration/dehydration reversible reactions. The model's main feature is that it treats rigorous phenomena occurring in the TChES unit. It accounts for local hygric and thermal non-equilibrium by treating heat and moisture carrier fluid and reactive porous bed separately. Therefore, two sets of governing equations have been derived, i.e., one dealing with moisture transfer in the air flowing through the porous bed and the second one with phenomena occurring in the reactive porous bed. The model can simulate the chemical and physical sorption process occurring in the TES unit.

Currently, the proposed model has been simplified and modified to simulate the sorption/desorption TES unit. It was implemented in 2D axisymmetric space by applying commercial software ANSYS Fluent and its advanced customization options, i.e., UDS, UDF, and UDM. The model was tested regarding the initial mesh size sensitivity and obeying mass and energy conservation principles. The obtained results were physical. It turned out that the current model implementation is very computationally inefficient, i.e., the computational time is very long. Therefore, only several minutes of the discharging and charging processes were simulated.

These problems with long simulation times were probably related to many couplings between different equations and properties, which are not necessarily required and have not necessarily meaningful impacts on the model's accuracy. But they could significantly decrease the convergence rates. So further work will be devoted to optimizing model implementation and improving convergence rates by decoupling model equations and properties and testing different numerical techniques for solving governing equations.

Acknowledgments

This work was financially supported by the National Science Centre (Poland) within project no. 2020/37/B/ST8/04021.

References

[1] Dincer I., Rosen M.A., Thermal energy storage: Systems and applications. Chichester, UK: Wiley; 2010.

[2] Darkwa K., Ianakiev A., O'Callaghan P.W., Modelling and simulation of adsorption process in a fluidised bed thermochemical energy reactor. Appl Therm Eng 2006;26:838-45.

[3] Torres Ledesma J., Łapka P., Domański R., Casares F.S., Numerical simulation of the solar thermal energy storage system for domestic hot water supply located in south Spain. Therm Sci 2013;17:431-42.

[4] Jaworski M., Łapka P., Furmański P., Numerical modelling and experimental studies of thermal behaviour of building integrated thermal energy storage unit in a form of a ceiling panel. Appl Energ 2014;113:548-57.

[5] Dydek K., Furmański P., Łapka P., Influence of PCMs in thermal insulation on thermal behaviour of building envelopes. J Phys Conf Ser 2016;745:032138.

[6] Łapka P., Jaworski M., Efficiency optimisation of the thermal energy storage unit in the form of the ceiling panel for summer conditions. Int J Energ Res 2019;43:2151-61.

[7] Kubiś M., Łapka P., Cieślikiewicz Ł., Sahmenko G., Sinka M., Bajare D., Analysis of the thermal conductivity of a bio-based composite made of hemp shives and a magnesium binder. Energies 2022;15:5490.

[8] N'Tsoukpoe K.E., Schmidt T., Rammelberg H.U., Watts B.A., Ruck W.K.L., A systematic multi-step screening of numerous salt hydrates for low temperature thermochemical energy storage. Appl Energ 2014;124:1-16.

[9] Mikos-Nuszkiewicz N., Furmański P., Łapka P., A mathematical model of charging and discharging processes in a thermochemical energy storage reactor using the hydrated potassium carbonate as a thermochemical material. Energy 2023;262:125642.

[10] Abedin A.H., Rosen M.A., Assessment of a closed thermochemical energy storage using energy and exergy methods. Appl Energ 2012;93:18-23.

[11] Neveu P., Tescari S., Aussel D., Mazet N., Combined constructal and exergy optimisation of thermochemical reactors for high temperature heat storage. Energ Convers Manage 2013;71:186-98.

[12] Albrecht K.J., Jackson G.S., Braun R.J., Thermodynamically consistent modeling of redox-stable perovskite oxides for thermochemical energy conversion and storage. Appl Energ 2016;165:285-96.

[13] Flegkas S, Birkelbach F, Winter F, Freiberger N, Werner A, Fluidized bed reactors for solid-gas thermochemical energy storage concepts – Modelling and process limitations. Energy 2018;143:615-23.

[14] Benoit M., Mazet N., Mauran S., Stitou D., Xu J., Thermochemical process for seasonal storage of solar energy: Characterization and modeling of a high density reactive bed. Energy 2012;47:553-63.

[15] Shao H, Nagel T, Roßkopf C, Linder M, Wörner A, Kolditz O, Non-equilibrium thermo-chemical heat storage in porous media: Part 2 – A 1D computational model for a calcium hydroxide reaction system. Energy 2013;60:271-82.

[16] Wang M., Chen L., Zhou Y., Tao W.Q., Numerical simulation of the physical-chemical-thermal processes during hydration reaction of the calcium oxide/calcium hydroxide system in an indirect reactor. Transport Porous Med 2021;140:667-96.

[17] Michel B., Neveu P., Mazet N., Comparison of closed and open thermochemical processes, for long-term thermal energy storage applications. Energy 2014;72:702-16.

[18] Ranjha Q., Oztekin A., Numerical analyses of three-dimensional fixed reaction bed for thermochemical energy storage. Renew Energ 2017;111:825-35.

[19] Shi T., Xu H., Qi C., Lei B., Wu Y., Zhao C., Multi-physics modeling of thermochemical heat storage with enhance heat transfer. Appl Therm Eng 2021;198:117508.

[20] Li W., Klemeš J.J., Wang Q., Zeng M., Numerical analysis on the improved thermo-chemical behaviour of hierarchical energy materials as a cascaded thermal accumulator. Energy 2021;232:120937.

[21] Rui J., Luo Y., Wang M., Peng J., She X., Design and performance evaluation of an innovative salt hydrates-based reactor for thermochemical energy storage. J Energy Storage 2022;55:105799.

 https://doi.org/10.52202/069564-0210